Chemical-order-dependent magnetic anisotropy and exchange stiffness constant of FePt (001) epitaxial films

S. Okamoto, N. Kikuchi, O. Kitakami, T. Miyazaki, and Y. Shimada
Institute of Multidisciplinary Research for Advanced Materials, Tohoku University, Sendai 980-8577, Japan

K. Fukamichi
Department of Materials Science, Graduate School of Engineering, Tohoku University, Sendai 980-8579, Japan
(Received 4 January 2002; published 8 July 2002)

Anomalous Hall voltage was measured for FePt $L1_0$ films having very high magnetic anisotropy. The magnetic anisotropy K_1 and K_2 were determined with high accuracy by analyzing the magnetization curves obtained from the Hall voltage measurement. The saturation magnetization M_s of the samples with different chemical-order parameter (S) exhibits a different temperature dependence, implying that the Curie temperature weakly depends on S. The first-order anisotropy K_1 gradually increases with S, while the second-order anisotropy K_2 remains almost constant of about 5×10^6 erg/cc. The temperature dependence of K_1 is correlated with S, that is, K_1 with a small S is more temperature dependent than that with a large S. These behaviors are quite similar to the temperature dependence of M_s with different S, and can be explained by the conventional model based on thermal spin fluctuations. The domain wall energy σ_w evaluated by the theoretical analysis of the stripe-domain structure tends to increase linearly with S, in a similar manner as that of K_1, whereas the exchange stiffness constant A of about 1×10^{-6} erg/cm deduced from σ_w and $K_u(=K_1+K_2)$ hardly depends on S.

DOI: 10.1103/PhysRevB.66.024413 PACS number(s): 75.30.Gw, 75.30.Et, 75.50.Bb, 75.60.Ch

I. INTRODUCTION

For the past few decades, magnetic recording has been a major technology of high-density information storage. In the near future, however, the so-called superparamagnetic limitation will emerge as a serious problem. To overcome this problem, intensive researches on materials having higher uniaxial magnetic anisotropy constant K_u than that of widely used CoCr-based alloys ($K_u\approx1\sim2\times10^6$ erg/cc)[1,2] have been carried out. The $L1_0$-type equiatomically ordered Fe(Co)Pt alloy is one of the most promising candidates as a new medium material because of its extremely high K_u of $4-10\times10^7$ erg/cc.[3–6] For this reason, extensive studies have been carried out on this alloy in the forms of epitaxially grown single-crystal films,[5–8] granular films,[9–11] chemically synthesized nanoparticles,[12] and isolated island particles.[13] Most of these researches have focused on the technological issues of high-density recording media, while the fundamental magnetic properties of Fe(Co)Pt $L1_0$, such as the temperature dependence of the magnetic anisotropy constants and the exchange stiffness constant, have been scarcely reported so far.

The first-principles calculations conclude that the strong K_u of Fe(Co)Pt $L1_0$ should be attributed to the large spin-orbit coupling of the Pt atom and hybridization of d bands between Fe(Co) and Pt atoms.[14,15] In addition, it should be emphasized that the marked feature of Fe(Co)Pt $L1_0$ is the structural anisotropy, that is, alternatively stacked Fe(Co) and Pt monolayers along the c axis. The uniaxial anisotropy K_u along the c axis that originates not only from the proximity effect between Fe(Co) and Pt atoms but also from the structural anisotropy is very similar to that of Fe/Pt and Co/Pt multilayers.[16,17] Experimentally, a strong dependence of K_u on the degree of chemical order and a slight enhancement of magnetization caused by transformation from the disordered state to the ordered state have been reported.[5] These results imply that the fundamental magnetic properties of Fe(Co)Pt $L1_0$ are very sensitive to the chemical-order. Further investigation of these properties, however, experimental difficulties such as preparation of a perfectly oriented $L1_0$ single crystal film and accurate determination of a very high K_u must be overcome.

In the present study, we have prepared and characterized high quality FePt $L1_0$ epitaxial films with various degree of chemical order and developed a simple method to measure and evaluate accurately the very high K_u. The magnetization and the magnetic anisotropy constants in association with the chemical order have been investigated. Furthermore, the domain wall energy and the exchange stiffness constant as a function of S have been determined.

II. EXPERIMENTS

The films were grown on MgO (100) single crystal substrates by dc magnetron sputtering. In the many of previous reports, a Pt or Cr buffer layer has been adopted to improve the crystal orientation of FePt $L1_0$.[6,7,17] However, atomic diffusion at the buffer/FePt interface is unavoidable during deposition or annealing at high temperatures. In the present study the films were directly deposited on the MgO (100), and perfect crystal orientation was available by seeking for the optimum deposition condition. The sputtering chamber was evacuated down to 3×10^{-8} Torr prior to film deposition and the sputtering gas pressure P_{Ar} was adjusted in the range from 1 to 10 mTorr. The substrate temperature T_s and FePt thickness d were adjusted in the range of 673–973 K and 110–490 Å, respectively. After deposition, a 20 Å thick

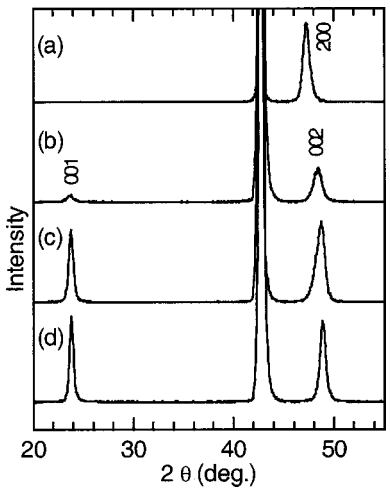

FIG. 1. XRD profiles for 200 Å thick FePt films grown at (a) substrate temperature $T_s = 673$ K and Ar pressure $P_{Ar} = 1$ mTorr, (b) $T_s = 673$ K and $P_{Ar} = 10$ mTorr, (c) $T_s = 973$ K and $P_{Ar} = 1$ mTorr, and (d) $T_s = 973$ K and $P_{Ar} = 10$ mTorr.

Pt protective layer was deposited at room temperature. The deposition rate for FePt was fixed within 22–24 Å/min. The film composition was confirmed to be equiatomic by using the energy-dispersive x-ray spectroscopy (EDX). The crystal structure was identified by the reflection high-energy electron diffraction (RHEED) and x-ray diffraction (XRD) with Cu-$K\alpha$ radiation. The chemical-order parameter S was defined as the probability of correct site occupation in the $L1_0$ lattice, and is given by the following Eq. (1):

$$S^2 = (I_{001}/I_{002})_{meas}/(I_{001}/I_{002})_{calc}, \quad (1)$$

where I_{001} and I_{002} are the integrated intensity of 001 superlattice and 002 fundamental diffractions and $(I_{001}/I_{002})_{meas}$ and $(I_{001}/I_{002})_{calc}$ are the measured and calculated diffraction intensity ratio, respectively. By taking the x-ray penetration depth[18] and Debye-Waller factor[7] into account, $(I_{001}/I_{002})_{calc}$ was calculated to be 2.0–1.9 for the film thickness ranging from 110 to 490 Å. The magnetizations were measured with a vibrating sample magnetometer (VSM) and a superconducting quantum interference device (SQUID). The magnetization loops were obtained by using the polar magneto-optical Kerr effect (PMOKE) and the anomalous Hall effect (AHE). The Hall effect measurement was carried out using a four probe ac resistance bridge at 980 Hz with a very low bias current of 10 μA. The magnetic domain structures were observed with a magnetic force microscope (MFM).

III. RESULTS AND DISCUSSION

A. Growth of FePt $L1_0(001)$

Figure 1 shows the $\theta-2\theta$ scans for 200 Å thick FePt films deposited at the substrate temperature $T_s = 673$ and 973 K. The Ar pressure P_{Ar} during sputtering was adjusted as 1 and 10 mTorr for each T_s. The XRD profiles for the samples grown at $T_s = 673$ K [Figs. 1(a) and 1(b)] clearly exhibit epitaxial growth of FePt on MgO (100), but no superlattice diffractions are observable in Fig. 1(a), indicating that the

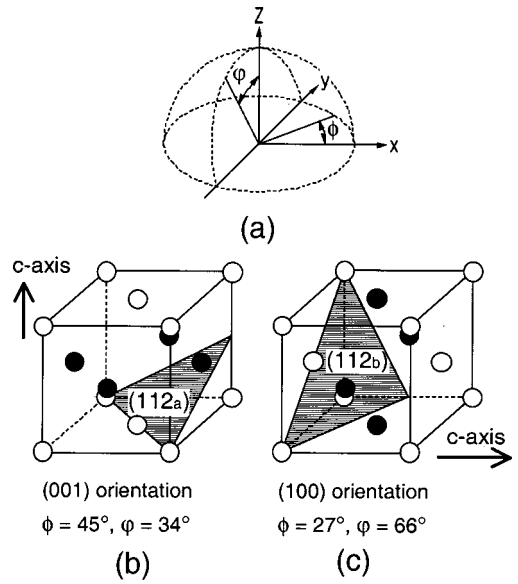

FIG. 2. (a) Schematic configuration of ϕ and φ for detection of FePt $L1_0$ 112 diffraction. ϕ and φ are the azimuthal and polar angle from MgO [100] and [001], respectively. X-ray incidence is in the x-z plane. (b) and (c) are illustrations of (112_a) and (112_b) shown as hatched areas in (001) and (100) orientations of FePt $L1_0$, respectively. The open and solid circles denote the Fe and Pt sites, respectively.

sample grown at $P_{Ar} = 1$ mTorr is in a perfectly disordered state, whereas the sample grown at $P_{Ar} = 10$ mTorr is partially ordered judging from the weak 001 superlattice diffraction in Fig. 1(b). Obviously adjusting the gas pressure is effective to enhance the chemical ordering, and a similar effect was also found in the samples grown at $T_s = 973$ K as shown in Figs. 1(c) and 1(d). These profiles exhibit strong 001 superlattice diffraction, indicating well ordered FePt $L1_0$. However, one may notice that the 002 fundamental diffraction from FePt grown at $P_{Ar} = 1$ mTorr [Fig. 1(c)] has an asymmetric shape spreading toward the lower angle, suggesting the presence of (100) variants. Since the peaks 002 and 200 are too close to each other to confirm the c axis orientation of FePt $L1_0$, we have investigated orientation of FePt $L1_0$ (112) with the XRD configuration illustrated in Fig. 2(a). By adjusting the azimuthal angle ϕ and the polar angle φ, FePt $L1_0$ (112) can meet the Bragg condition. The condition is satisfied at $\phi \approx 45°$ and $\varphi \approx 34°$ for (001) orientation and $\phi \approx 27°$ and $\varphi \approx 66°$ for (100) orientation, which are denoted as (112_a) and (112_b) in Figs. 2(b) and 2(c). Figure 3 presents 112_a and 112_b diffraction profiles of the samples given in Fig. 1. No 112_b diffractions is detected in the samples grown at $P_{Ar} = 10$ mTorr as seen in Figs. 3(b) and 3(d), indicating that deposition under high Ar pressure promotes the chemical ordering as well as the c axis orientation.

Suzuki *et al.* have observed a similar phenomenon that is accompanied by an appreciable decrease of the lattice spacing of FePt (001) with increase of sputtering gas pressure.[19] They inferred that vertical compressive stress during sputtering affects chemical ordering and c axis orientation in FePt $L1_0$. However, these phenomena should be attributed to a

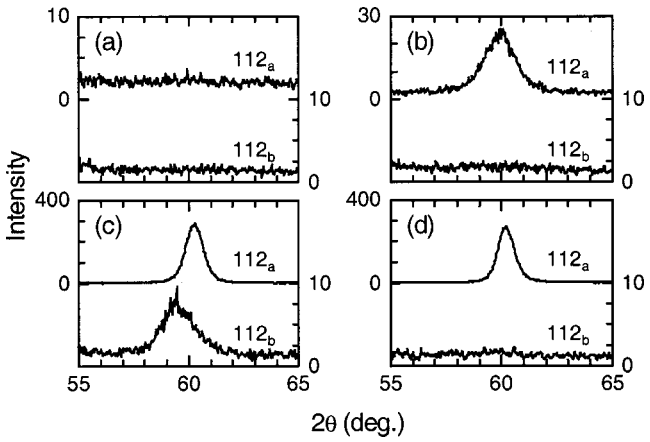

FIG. 3. XRD profiles of 112_a (upper) and 112_b diffractions (bottom) for 200 Å thick FePt films grown at (a) substrate temperature $T_s = 673$ K and Ar pressure $P_{\mathrm{Ar}} = 1$ mTorr, (b) $T_s = 673$ K and $P_{\mathrm{Ar}} = 10$ mTorr, (c) $T_s = 973$ K and $P_{\mathrm{Ar}} = 1$ mTorr, and (d) $T_s = 973$ K and $P_{\mathrm{Ar}} = 10$ mTorr.

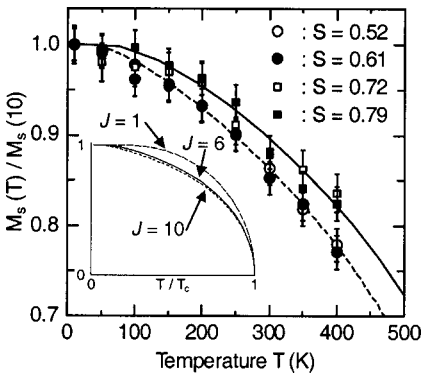

FIG. 4. Temperature dependence of normalized magnetization $M_s(T)/M_s(10)$ for 140 Å thick FePt films with the chemical-order parameter $S = 0.52$, 0.61, 0.72, and 0.79. The solid and broken lines are the calculated $M_s(T)/M_s(0)$ curves using the Brillouin function within the molecular field approximation for the momentum quantum number $J = 6$ and the Curie temperature $T_c = 750$ K and for $J = 10$ and $T_c = 700$ K. The inset shows the calculated $M_s(T)/M_s(0)$ vs T/T_c curves for $J = 1$, 6, and 10.

natural bilayer stacking growth observed in various thin films.[20–22] The natural bilayer stacking has been originally found at the surface of several binary alloys, such as Ni-Pt,[23] Ni-Ag,[24] and Co-Pt.[25] The periodic compositional modulation in several layers at these alloy surface has been observed and explained by the size mismatch and surface tension effects.[26,27] Recently, using molecular beam epitaxy (MBE), a new type stacked hcp superlattice has been reported for Co-Pt (Refs. 20 and 21) and Co-Ru,[22] which is caused by a alternative segregation on the advancing surface during thin film growth. This is the reason for the preferential *c* axis orientation in epitaxial FePt $L1_0$ on MgO (100), because Fe and Pt monolayers are alternatively stacked along the *c* axis in FePt $L1_0$. However, the natural stacking process along the film growth direction is severely disturbed by bombardment of high-energy particles.[28] This is the reason why the long-range ordering is attained more easily by MBE than the sputtering process.[29] A similar discussion is valid for the sputtering gas pressure effect in the present experiment, where the high Ar gas pressure decreases the kinetic energy of incident particles due to frequent collisions in the plasma space. All the samples for further study are the ones deposited at $P_{\mathrm{Ar}} = 10$ mTorr, which have excellent *c* axis orientation as confirmed by the XRD measurements mentioned above.

B. Magnetic anisotropy

Regardless of the order parameter *S* which varies in the range of 0.4–0.9, the magnetization M_s of all FePt $L1_0$ films is 1100 ± 100 emu/cc at room temperature which coincides with the value of bulk FePt $L1_0$,[4] and no significant difference is observed. On the other hand, the temperature dependence of the magnetization is sensitive to the parameter *S*. Shown in Fig. 4 is temperature dependence of the saturation magnetization $M_s(T)$ for 140 Å thick FePt films with $S = 0.52$, 0.61, 0.72, and 0.79. Note that the samples with smaller *S* exhibit a faster decrease of M_s with *T*. The solid and broken lines are the fitting results using the Brillouin function within a framework of the molecular field approximation.[30] The fitting parameters are the momentum quantum number *J* and the Curie temperature T_c. The best fitting was obtained with $J = 6$ and $T_c = 750$ K for the larger *S* of 0.72 and 0.79 and $J = 10$ and $T_c = 700$ K for the smaller *S* of 0.52 and 0.61. The Curie temperature of 750 K for the larger *S* coincides with the reported value of the bulk FePt $L1_0$.[31] The values of *J* assumed in the fitting calculations are much larger than that usually used for Fe ($J = 1$). The anomalously large value of *J* in the molecular field approximation have been reported for several materials,[2,32] not literally indicating the large magnetic moment, because this approximation is based on the one-body model. As is well known, the larger *J* becomes, the more sensitively the $M_s(T)/M_s(0) - T/T_c$ curve in the molecular field approximation, as seen from the inset in Fig. 4. If the decrease of $M_s(T)$ at low temperatures is attributed to the spin wave excitation, the exchange stiffness constant *A* should be inversely proportional to the coefficient of $T^{2/3}$ law.[32] This implies that the constant *A* in FePt $L1_0$ is much smaller than that in Fe and weakly dependent on *S*. Experimental and quantitative discussions on *A* of FePt $L1_0$ will be given in Sec. III C.

Because of the extremely high anisotropy field H_k of about 100 kOe, the accurate determination of anisotropy constants of FePt $L1_0$ is difficult by the conventional methods such as torque curve analyses[5,7] and the magnetization curve along the hard axis.[6] In the previous works, both of these methods have been carried out in external fields much lower than H_k.[5–7] Measurements in low fields may cause serious errors in evaluation and separation of the anisotropy constants, K_1, K_2,..., in the uniaxial anisotropy energy expression $E(\theta) = K_1 \sin^2\theta + K_2 \sin^4\theta + \cdots$, where θ denotes the angle of magnetization with respect to the easy axis.[33] In the present work, these constants are determined from the anomalous Hall effect, because it gives the magnetization vector along the film normal with very high sensitivity without no background signals from diamagnetism of a substrate

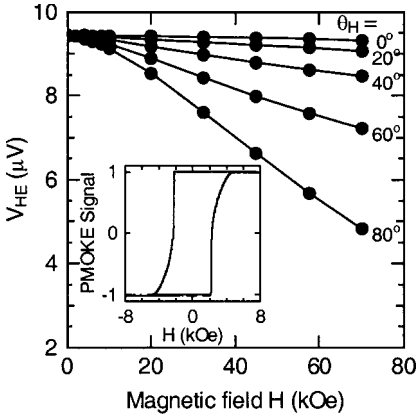

FIG. 5. V_{HF}-H curves for a 140 Å thick FePt film with the chemical-order parameter $S=0.72$ as a function of field direction θ_H. The inset is a PMOKE loop.

or a sample holder. By using the generalized Sucksmith-Thompson (GST) method[34] the anisotropy constants K_1 and K_2 were accurately determined by analysis of the magnetization curve from the Hall effect. The GST is an improvement of Sucksmith-Thompson (ST) method.[33,35] Formation of reversed domains during the magnetization process can be completely inhibited by the field component along the film normal, as will be described below.[34] In addition to the high accuracy mentioned above, it should be stressed that a very high field to saturate the sample is not required in the GST method.

The Hall voltage V_{HE} in a magnetic film is given by[36]

$$V_{HE}=V_{NHE}+V_{AHE}, \tag{2}$$

where V_{NHE} and V_{AHE}, respectively, denote the normal and the anomalous Hall voltages, and are expressed as

$$V_{NHE}=\frac{R_0 I}{d}H_z, \quad H_z=\cos\theta_H \tag{3}$$

and

$$V_{AHE}=\frac{R_s I}{d}M_z, \quad M_z=M_s\cos\theta_M, \tag{4}$$

where R_0 and R_s are the normal and the anomalous Hall coefficients, respectively, θ_H and θ_M are the directions of the external field H and the magnetization M_s from the film normal, d is the film thickness, and I is the current flow in the sample. Since R_s is much larger than R_0 for FePt (Refs. 37 and 38) and V_{NHE} is negligibly small for θ_H close to 90°, V_{HE} is nearly equal to V_{AHE}. Consequently, V_{HE}-H curves coincide with M_z-H. Shown in Fig. 5 are typical V_{HE}-H curves for a 140 Å thick FePt film with $S=0.72$ when the field is decreased from 70 to 0 kOe. The M-H loop in the inset measured by PMOKE has a good squareness, giving an evidence that the magnetic easy axis is parallel to the c axis. The point to be noted in Fig. 5 is that all V_{HE} measured at various θ_H converge on the same value at $H=0$. These results apparently indicate that, regardless of θ_H, the magnetization maintains the uniform rotation process without any reversed domains during the measurement.

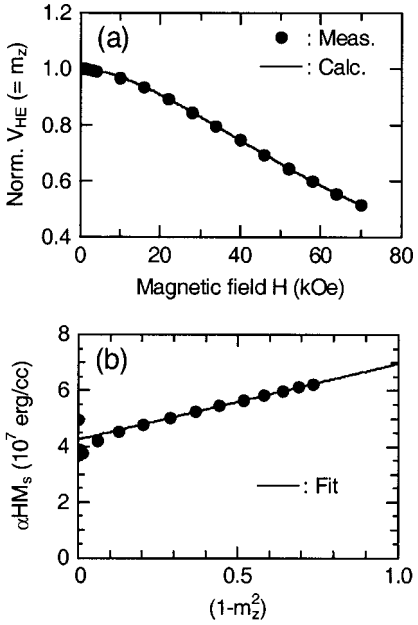

FIG. 6. (a) Normalized V_{HE}-H curve measured at $\theta_H=80°$ for a 140 Å thick FePt film with the chemical-order parameter $S=0.72$. (b) αHM_s vs $(1-m_z^2)$. The V_{HE} curve in (a) is replotted using the equilibrium relation Eq. (5) in the text. The solid line in (a) is the calculated m_z curve using K_1^{eff} and K_2 determined from intersection with the ordinate and the slope of the fitted line in (b).

The magnetic anisotropy constants of the films can be determined by analyzing the normalized V_{HE} curves by the GST method. From the equilibrium magnetization condition, the relation is deduced as[34]

$$2K_1^{eff}+4K_2(1-m_z^2)=\alpha HM_s, \tag{5}$$

with

$$\alpha=\frac{m_z\sin\theta_H-\sqrt{1-m_z^2}\cos\theta_H}{m_z\sqrt{1-m_z^2}},$$

where m_z is the normalized M_z, K_1^{eff} includes K_1 and the demagnetizing energy $2\pi M_s^2$. By plotting αHM_s vs $(1-m_z^2)$, one can determine both K_1^{eff} and K_2. A representative result is shown in Fig. 6(a), where the normalized V_{HE} $(=m_z)$ curve was measured at $\theta_H=80°$ for a 140 Å thick FePt film with $S=0.72$. By replotting the data in Fig. 6(a) in accordance with Eq. (5), we can obtain the αHM_s vs $(1-m_z^2)$ curve as given in Fig. 6(b). From intersection with the ordinate and the slope of the curve, K_1^{eff} and K_2 are determined as $K_1^{eff}=2.13\pm0.06\times10^7$ erg/cc and $K_2=6.7\pm0.7\times10^6$ erg/cc. What has to be stressed here is that the thus determined anisotropy constants perfectly reproduce the experimental V_{HE}-H curve as shown by the solid line in Fig. 6(a), indicating that the magnetization uniformly rotates as mentioned above.

The chemical-order dependence of K_1 and K_2 was measured at room temperature for the 140 Å thick FePt films as

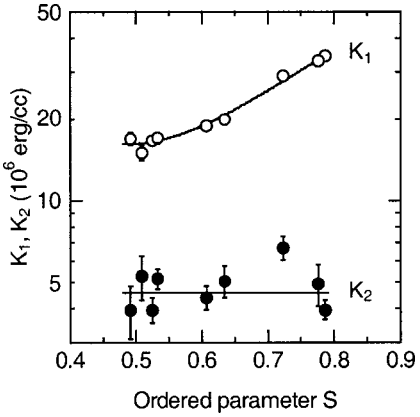

FIG. 7. The first- and the second-order uniaxial anisotropy constants K_1 and K_2 at room temperature for 140 Å thick FePt films as a function of chemical-order parameter S. The solid lines are guides to the eye.

shown in Fig. 7. With increasing S, K_1 gradually increases in agreement with the previous report,[5] whereas K_2 remains almost constant and is about 5×10^6 erg/cc. The data of the other samples with thickness of 110–490 Å exhibit similar to the results given in Fig. 7. Moreover, the temperature dependences of K_1 and K_2 were investigated, and is shown in Fig. 8. The values of K_1 and K_2 for the 140 Å thick sample with $S=0.72$ decrease monotonically with temperature. Figure 9(a) summarizes the temperature dependence of $K_1(T)$ normalized to the values at 10 K for the samples with $S=0.52$, 0.61, 0.72, and 0.79. The smaller S the more sensitive the temperature dependence of K_1, similar to the temperature dependence of M_s.

According to the theory within the framework of thermal fluctuations of magnetic moments,[39,40] the temperature dependence of K_1 is expressed as

$$K_1(T)/K_1(0)\approx[M_s(T)/M_s(0)]^{n(n+1)/2}, \qquad (6)$$

with $n=2$ for the first-order uniaxial anisotropy constant. The log-log plot of $K_1(T)/K_1(10)$ vs $M_s(T)/M_s(10)$ obtained from Fig. 9(a) is presented in Fig. 9(b). All $K_1(T)$

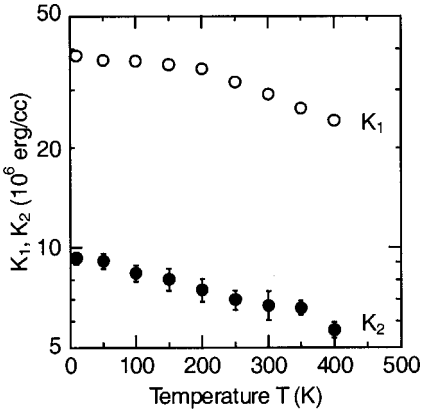

FIG. 8. Temperature dependence of the first- and the second-order uniaxial anisotropy constants K_1 and K_2 for a 140 Å thick FePt film with the chemical-order parameter $S=0.72$.

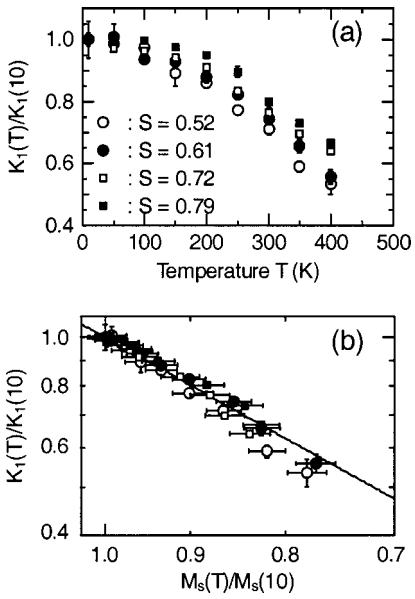

FIG. 9. (a) Temperature dependences of $K_1(T)/K_1(10)$ for 140 Å thick FePt films with the chemical-order parameter $S=0.52$, 0.61, 0.72, and 0.79. (b) log-log plot of $K_1(T)/K_1(10)$ vs $M_s(T)/M_s(10)$. The solid line in (b) is least-square fitting with a slope of 2.1.

data for various S fall on the same straight line, implying that the temperature dependence of K_1 of FePt $L1_0$ can be treated by the model mentioned above. Strictly, the slope in Fig. 9(b) is about 2.1, that is smaller than 3 expected from $n=2$, and a slight deviation from the linear relation is seen in the high temperature region $T\geqslant300$ K. This deviation suggests that the presence of other contributions such as thermal lattice expansion and/or the higher order anisotropy.[40]

C. Domain structure and exchange stiffness

Figures 10(a), 10(b), and 10(c) demonstrate MFM images for the 110, 210, and 320 Å thick FePt films with $S=0.4$–0.5, and (d) is an illustration of the stripe-domain structure. After ac demagnetization, very clear stripe domains with a period of $L\approx2000$ Å were observed in the films thicker than 200 Å. While for $d<200$ Å, the structure abruptly changes from the well defined stripe domains to irregular and larger domains. Variation of the domain period L with d for the samples with nearly the same S of 0.4–0.5, $K_1=1.0\sim1.5\times10^7$ erg/cc, and K_2 of 5×10^6 erg/cc is shown in Fig. 11. We see that L decreases very gradually with d. This change of L is closely related with the magnetization process of the FePt $L1_0$ films. Shown in Fig. 12(a) is the initial magnetization curve along the film normal after ac demagnetization for the same sample given in Fig. 10(c). The magnetization increases very gradually up to a certain field H_p, and linearly increases above H_p. Below H_p, pinning sites such as grain boundaries hinder the domain wall displacement. The domains with the magnetization direction opposite to the external field shrink with increasing the field above $H\geqslant H_p$. For further increase of the field the stripe-domain structure changes into bubble domains, as commonly

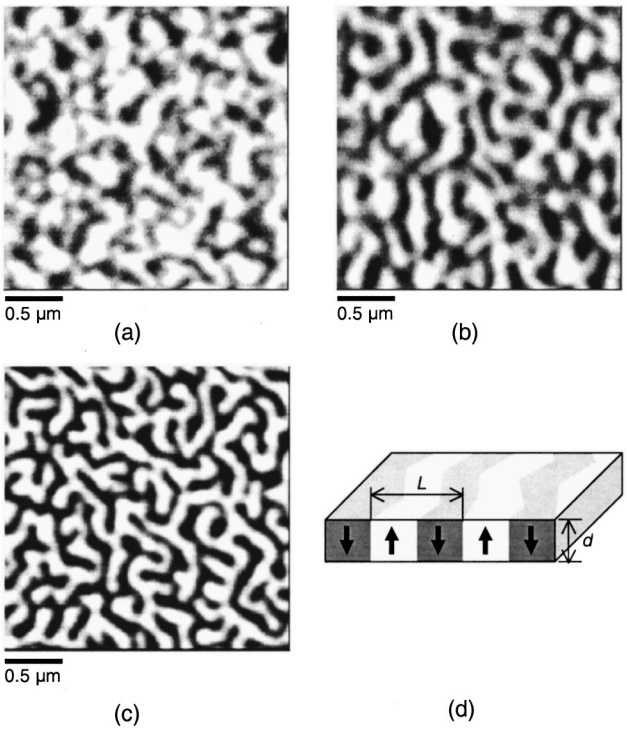

FIG. 10. MFM images for (a) 110 Å, (b) 210 Å, and (c) 320 Å thick FePt films with the chemical-order parameter $S=0.4-0.5$. (d) is an illustration of the stripe-domain structure. L and d are the domain period and the film thickness, respectively. The thick arrows indicate the magnetization direction in the domains.

observed in perpendicular magnetization films.[41] In the analysis of the stripe-domain behavior in FePt $L1_0$ films, we define two kinds of saturation fields H_{S1} and H_{S2} $(=H_{S1}-H_p)$ by extrapolating the linear part of the magnetization curve as given in Fig. 12(a). Figure 13 shows H_{S1} and H_{S2} as functions of film thickness d for the samples given in Fig. 11. Both H_{S1} and H_{S2} rapidly increase with increasing d above 200 Å.

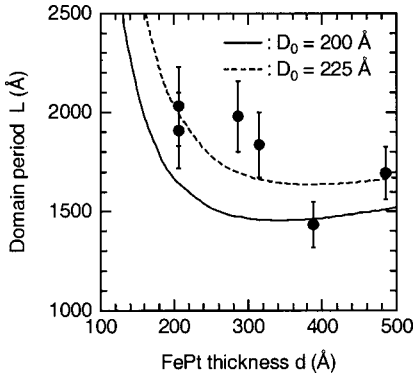

FIG. 11. The domain period L as a function of d for the FePt films having the chemical-order parameter $S=0.4-0.5$ ($K_1=1.0\sim1.5\times10^7$ erg/cc, $K_2\approx5\times10^6$ erg/cc). The solid and broken line are the calculated domain period L^{calc} assuming the dipolar length $D_0=200$ and 225 Å, respectively.

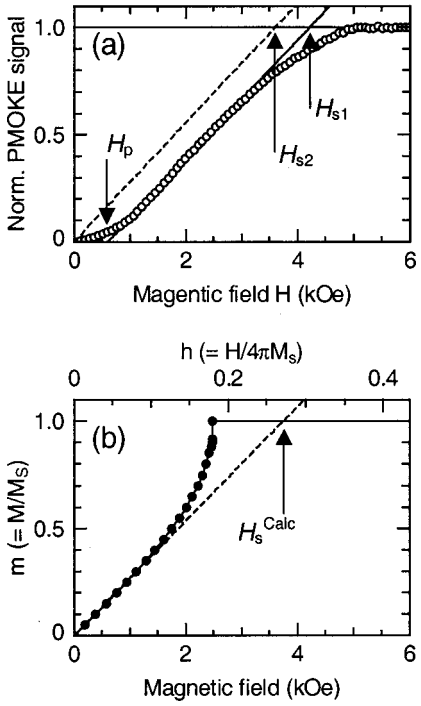

FIG. 12. (a) Initial magnetization curve (open circles) for a 320 Å thick FePt film with the chemical-order parameter $S=0.52$. (b) Calculated magnetization curve (solid circles) for the reduced field $(h=H/4\pi M_s)$ assuming $D_0=230$ Å, $d=320$ Å, and $K_u=1.5\times10^7$ erg/cc.

We analyze these behaviors by using the domain theory given by Kooy and Enz.[41] The characteristic length, or the so-called dipolar length,[42] is defined as

$$D_0=\sigma_w/2\pi M_s^2, \tag{7}$$

where σ_w is the wall energy density per unit area. Physically D_0 is the measure for the critical thickness between single- and multiple-domain states, as originally discussed by Kittel.[43] Kooy and Enz[41] derived the analytical expression for the magnetization process of stripe-domain structures as-

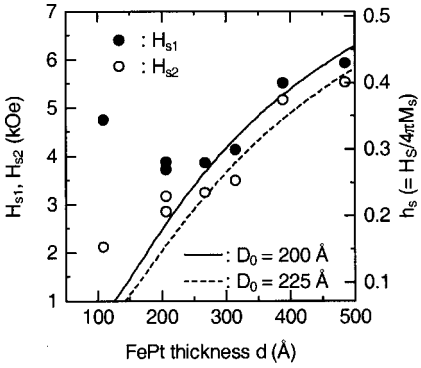

FIG. 13. Thickness dependence of the saturation fields H_{s1} and H_{s2} for FePt films with the chemical-order parameter $S=0.4\sim0.5$ ($K_1=1.0\sim1.5\times10^7$ erg/cc, $K_2\approx5\times10^6$ erg/cc). The solid and dashed line are the calculated saturation field H_s^{calc} for the dipolar length $D_0=200$ and 225 Å, respectively. The right-hand ordinate is the corresponding reduced saturation field $(h_s=H_s/4\pi M_s)$.

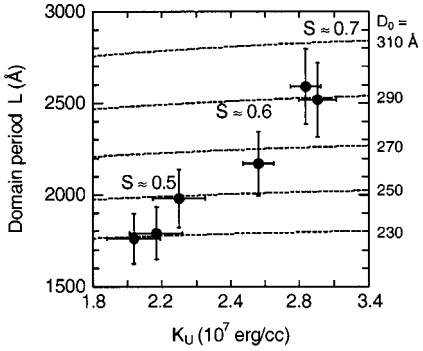

FIG. 14. Domain period L vs the uniaxial anisotropy constant K_u $(=K_1+K_2)$ for 290 Å thick FePt films. The broken lines stand for the calculated domain period L^{calc} assuming various dipolar lengths D_0.

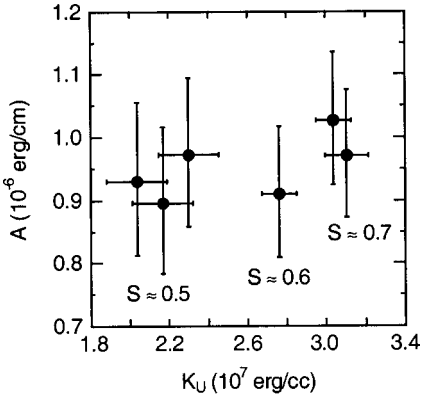

FIG. 16. The exchange stiffness constant A vs the uniaxial anisotropy constant K_u $(=K_1+K_2)$ for a 290 Å thick FePt film.

suming $d \gg D_0$. However, this assumption is invalid for the thickness range of the present samples, and hence we have carried out more rigorous calculation without the assumption mentioned above. The total energy e_t in this calculation includes the wall energy e_w, the applied field energy e_h and the demagnetization energy e_d. Each energy normalized to the maximum demagnetizing energy $2\pi M_s^2$ is expressed as

$$e_w = \frac{2D_0}{L} = \frac{2D_0\beta}{d\sqrt{\mu}}, \tag{8}$$

$$e_h = 2hm, \tag{9}$$

$$e_d = m^2 + \frac{8\sqrt{\mu}}{\pi^3\beta}\sum_n \frac{1}{n^3}\sin^3\left[\frac{n\pi}{2}(1+m)\right]\frac{\sinh(n\pi\beta)}{\sinh(n\pi\beta)+\sqrt{\mu}\cosh(n\pi\beta)}, \tag{10}$$

where $m=M/M_s$, $h=H/4\pi M_s$, $\beta=d\sqrt{\mu}/L$, and $\mu=1+2\pi M_s^2/K_u$. The energy minimum conditions of $\partial e_t/\partial\beta=0$ and $\partial e_t/\partial m=0$ give the equilibrium values of L and m. The magnetization thus calculated using the parameters of $D_0=230$ Å, $d=320$ Å, and $K_u=1.5\times10^7$ erg/cc is shown with solid circles in Fig. 12(b). The shape of the calculated curve is obviously different from the measured one, especially near the saturation region. This is because the calculation ignores formation of bubbles near the saturation region.[41] Therefore, we predict the saturation field H_S^{calc} by extrapolating the linear part of the calculated curve as depicted in Fig. 12(b). By assuming a proper value for D_0 together with the experimental K_u $(=K_1+K_2\approx1.5\times10^7$ erg/cc), we can reproduce accurately the measured H_{S1} and H_{S2}, as shown by the solid and broken lines for $D_0=200$ and 225 Å in Fig. 13. The calculated domain period L^{calc} in the demagnetized state with D_0 as a parameter is given in Fig. 11. It is noteworthy that L^{calc} for $D_0=225$ Å is in good agreement with the experimental L. As a result, the experimental saturation field H_{S2}, which eliminates the effect of wall pinning, and the domain period L are consistently reproduced by assuming the parameter D_0 to be 225 Å. From the analyses of the FePt films with the same order of K_u, it has been confirmed that the stripe-domains of FePt $L1_0$ are correctly described with Kooy and Enz's theory.[41] Then, we will use this theoretical relation among L, K_u, and D_0 to figure out how the degree of chemical order of FePt $L1_0$ affects the wall energy σ_w and the exchange stiffness constant A.

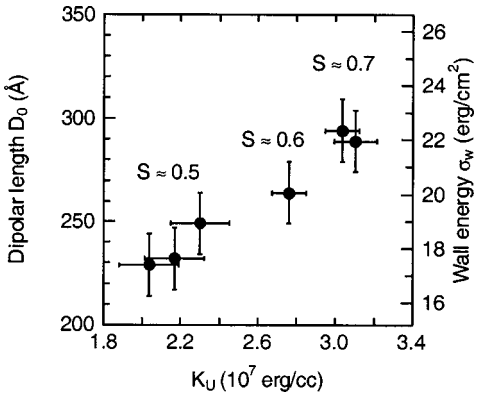

FIG. 15. Dipolar length D_0 as a function of the uniaxial anisotropy constant K_u $(=K_1+K_2)$ for 290 Å thick FePt films. The right-hand ordinate is the corresponding wall energy σ_w.

The relationship between the measured L and K_u $(=K_1+K_2)$ for the 290 Å thick samples with various S is given in Fig. 14. The broken lines indicate L^{calc} calculated assuming various D_0. The assumed D_0 which coincide with the experimental L and K_u are plotted in Fig. 15. The right-hand ordinate indicates the corresponding wall energy σ_w derived from Eq. (7). The values of D_0 of FePt $L1_0$ evaluated here are much smaller than the previous data of about 500 Å by Thiele *et al.*[7] They derived D_0 by using the theoretical model[44] calculated by Kaplan *et al.*,[42] assuming $d \ll D_0$. However, their FePt thickness ranged 1000–2000 Å, far from the thickness range valid for Kaplan's assumption.[42,44] The exchange stiffness constant A versus K_u is shown in Fig. 16, in which A was derived assuming the 180° Bloch-type wall energy expressed as

$$\sigma_w = 4\sqrt{AK_u}. \tag{11}$$

The value of $A \approx 1 \times 10^{-6}$ erg/cm is much smaller than that of Fe$\approx 2 \times 10^{-6}$ erg/cm,[45] and almost independent of K_u. This fact is consistent with the larger temperature dependence of M_s discussed in Sec. III B. Although there seems to be a slight dependence of A on K_u in Fig. 16, it is almost within the experimental error of $\pm 0.1 \times 10^{-6}$ erg/cm.

IV. SUMMARY

We have fabricated fully orientated equiatomic FePt $L1_0$ (001) films on MgO (100) substrates. Using these specimens the basic magnetic propertied, namely, the magnetic anisotropy constants K_1 and K_2, their temperature dependence, and the exchange stiffness constant A, have been investigated in correlation with the degree of chemical order.

The sputter deposition under higher Ar pressures promoted the chemical order as well as its c axis orientation of FePt $L1_0$, and perfectly orientated FePt $L1_0$ (001) films were obtained at Ar pressure of 10 mTorr.

The FePt films with different chemical-order parameters S exhibit a different temperature dependence of saturation magnetization M_s. At low temperatures and for small S it tends to decrease rapidly with increasing temperature. The first- and second-order magnetic anisotropy constants K_1 and K_2 were accurately determined from the generalized Sucksmith-Thompson's method using magnetization curves obtained by the anomalous Hall effect. The value of K_1 gradually increases with S, whereas K_2 is insensitive to S. The temperature dependence of K_1 is larger for smaller S. This temperature dependence is similar to that of M_s and is explained by the thermal spin fluctuation.

The experiments and the analysis of the stripe-domain structures with the film thickness as a parameter under the condition of constant K_u revealed that the domain structure is consistent with the model by Kooy and Enz. By using this consistent relation the dipolar length D_0 was evaluated by measured L for the films with the same thickness but different K_u and S. The exchange stiffness constant A derived from the experimental K_u and D_0 has little correlation with K_u and S.

ACKNOWLEDGMENTS

The present work has been supported by the Research for the Future Program, Grant No. 97R14701, and Grant-in-Aid for Scientific Research from the Japan Society for the Promotion of Science, and the Storage Research Consortium in Japan.

[1] O. Kitakami, N. Kikuchi, S. Okamoto, Y. Shimada, K. Oikawa, Y. Otani, and K. Fukamichi, J. Magn. Magn. Mater. **202**, 305 (1999).
[2] N. Inaba, Y. Uesaka, and M. Futamoto, IEEE Trans. Magn. **36**, 54 (2000).
[3] V. V. Maykov, A. Ye. Yermakov, G. V. Ivanov, V. I. Khrabrov, and L. M. Magat, Fiz. Met. Metalloved. **67**, 79 (1989).
[4] O. A. Ivanov, L. V. Solina, V. A. Demshina, and L. M. Magat, Fiz. Met. Metalloved. **35**, 92 (1973).
[5] H. Kanazawa, G. Lauhoff, and T. Suzuki, J. Appl. Phys. **87**, 6143 (2000).
[6] R. F. C. Farrow, D. Weller, R. F. Marks, M. F. Toney, A. Cebollada, and G. R. Harp, J. Appl. Phys. **79**, 5967 (1996).
[7] J.-U. Thiele, L. Folks, M. F. Toney, and D. K. Weller, J. Appl. Phys. **84**, 5686 (1998).
[8] M. R. Visokay and R. Sinclair, Appl. Phys. Lett. **66**, 1692 (1995).
[9] C. P. Luo and D. J. Sellmyer, Appl. Phys. Lett. **75**, 3162 (1999).
[10] M. Watanabe, T. Masumoto, D. H. Ping, and K. Hono, Appl. Phys. Lett. **76**, 3971 (2000).
[11] C. Chen, O. Kitakami, and Y. Shimada, IEEE Trans. Magn. **35**, 3466 (1999); C. Chen, O. Kitakami, S. Okamoto, and Y. Shimada, J. Appl. Phys. **87**, 6947 (2000).
[12] S. Sun, C. B. Murray, D. Weller, L. Folks, and A. Moser, Science **287**, 1989 (2000).
[13] H. Sakaue, T. Miyazaki, O. Kitakami, and Y. Shimada, J. Magn. Soc. Jpn. **25**, 847 (2001).
[14] A. Sakuma, J. Phys. Soc. Jpn. **63**, 3054 (1994).
[15] G. H. O. Daalderop, P. J. Kelly, and M. F. H. Schuurmans, Phys. Rev. B **44**, 12 054 (1991).
[16] K. Kyuno, R. Yamamoto, and S. Asano, J. Phys. Soc. Jpn. **61**, 2099 (1992).
[17] L. Szunyogh, P. Weinberger, and C. Sommers, Phys. Rev. B **60**, 11 910 (1999).
[18] S. Okamoto, O. Kitakami, and Y. Shimada, J. Magn. Magn. Mater. **208**, 102 (2000).
[19] T. Suzuki, K. Harada, N. Honda, and K. Ouchi, J. Magn. Magn. Mater. **193**, 85 (1999).
[20] G. R. Harp, D. Weller, T. A. Rabedeau, R. F. C. Farrow, and M. F. Toney, Phys. Rev. Lett. **71**, 2493 (1993).
[21] M. Maret, M. C. Cadeville, A. Herr, R. P. Poinsot, E. Beaurepaire, S. Lefebvre, and M. Bessiére, J. Magn. Magn. Mater. **191**, 61 (1999).
[22] L. Bouzidi, V. Pierron-Bohnes, O. Haemmerlé, C. Bouillet-Ulhaq, and M. C. Cadeville, Thin Solid Films **318**, 215 (1998).
[23] Y. Gauthier, Y. Joly, R. Baudoing, and J. Rundgren, Phys. Rev. B **31**, 6216 (1985); R. Baudoing, Y. Gauthier, M. Lundberg, and J. Rundgren, J. Phys. C **19**, 2825 (1986).
[24] A. Rolland and B. Aufray, Surf. Sci. **162**, 530 (1985).
[25] Y. Gauthier, R. Baudoing-Savois, J. M. Bugnard, U. Bardi, and A. Atrei, Surf. Sci. **276**, 1 (1992).
[26] G. Tréglia and B. Legrand, Phys. Rev. B **35**, 4338 (1987).
[27] M. Landberg, Phys. Rev. B **36**, 4692 (1987).
[28] C. Sürgers, E. Kay, and X. Wang, J. Appl. Phys. **80**, 5753 (1996).
[29] P. Caro, A. Cebollada, F. Briones, M. F. Toney, J. Cryst. Growth **187**, 426 (1998).
[30] S. Chikazumi, *Physics of Ferromagnetism*, 2nd ed. (Clarendon Press, Oxford, 1997).
[31] L. Graf and A. Kussmann, Phys. Z. **36**, 544 (1935).
[32] Y. Sugita, H. Takahashi, M. Komuro, M. Igarashi, R. Imura, and T. Kambe, J. Appl. Phys. **79**, 5576 (1996).
[33] Y. Endo, O. Kitakami, S. Okamoto, and Y. Shimada, Appl. Phys. Lett. **77**, 1689 (2000).

[34] S. Okamoto, K. Nishiyama, O. Kitakami, and Y. Shimada, J. Appl. Phys. **90**, 4085 (2001).
[35] W. Sucksmith and J. E. Thompson, Proc. R. Soc. London, Ser. A **225**, 362 (1954).
[36] S. de Haan, C. Lodder, and T. J. A. Popma, J. Magn. Soc. Jpn. **15(S2)**, 349 (1991).
[37] C. L. Canedy, G. Q. Gong, J. Q. Wang, and G. Xiao, J. Appl. Phys. **79**, 6126 (1996).
[38] M. Watanabe, T. Iwasa, and T. Masumoto, J. Magn. Soc. Jpn. **24**, 543 (2000); M. Watanabe and T. Masumoto, Thin Solid Films **405**, 92 (2002).
[39] C. Zener, Phys. Rev. **96**, 1335 (1954).
[40] W. J. Carr, Jr., Phys. Rev. **109**, 1971 (1958).
[41] C. Kooy and U. Enz, Philips Res. Rep. **15**, 7 (1960).
[42] B. Kaplan and G. A. Gehring, J. Magn. Magn. Mater. **128**, 111 (1993).
[43] C. Kittel, Phys. Rev. **70**, 965 (1946).
[44] V. Gahanno, Y. Samson, A. Marty, B. Gilles, and A. Chamberod, J. Magn. Magn. Mater. **172**, 26 (1997).
[45] T. G. Phillips, Phys. Lett. **17**, 11 (1965).